Dysregulation of Nrf2/Keap1 redox pathway in diabetes affects multipotency of stromal cells

Running title: Dysregulated of Nrf2/Keap1affects stromal cells

Piul S. Rabbani[1*], Marc A. Soares[1], Sophia G. Hameedi[1], Rohini L. Kadle[1], Adnan Mubasher[1], Maria Kowzun[1], Daniel J. Ceradini[1]*

1. Hansjörg Wyss Department of Plastic Surgery, New York University School of Medicine, New York, NY 10016

*Correspondence:

Piul S. Rabbani

Hansjörg Wyss Department of Plastic Surgery

New York University School of Medicine, New York, NY 10016

212-263-8745

piul.rabbani@nyumc.org

Daniel J. Ceradini

Hansjörg Wyss Department of Plastic Surgery

New York University School of Medicine, New York, NY 10016

212-263-8745

daniel.ceradini@nyumc.org

Word Count: 4585

Number of Figures: 7

Abstract

The molecular and cellular level reaches of the metabolic dysregulations that characterize diabetes are yet to be fully discovered. As mechanisms underlying management of reactive oxygen species (ROS) gain interest as crucial factors in cell integrity, questions arise about the role of redox cues in regulation and maintenance of bone marrow-derived multipotent stromal cells (BMSCs) that contribute to wound healing, particularly in diabetes. Through comparison of BMSCs from wild type and diabetic mice, with a known redox and metabolic disorder, we found that the cytoprotective Nrf2/Keap1 pathway is dysregulated and functionally insufficient in diabetic BMSCs. Nrf2 is basally active, but in chronic ROS we found irregular inhibition of Nrf2 by Keap1, altered metabolism and limited BMSC multipotency. Forced upregulation of Nrf2-directed transcription, through knockdown of Keap1, restores redox homeostasis. Normalized Nrf2/Keap1 signaling restores multipotent cell properties in diabetic BMSCs through Sox2 expression. These restored BMSCs can resume their role in regenerative tissue repair and promote healing of diabetic wounds. Knowledge of diabetes and hyperglycemia-induced deficits in BMSC regulation, and strategies to reverse them offers translational promise. Our study establishes Nrf2/Keap1 as a cytoprotective pathway, as well as a metabolic rheostat that affects cell maintenance and differentiation switches in BMSCs.

Introduction

Addressing the clinical manifestations of type II diabetes and associated complications, such as chronic non-healing wounds, necessitates a thorough understanding of pathological molecular and cellular events. Oxidative stress and flawed redox mechanisms induce metabolic deficiencies in diabetes and give rise to the characteristic insulin resistance (1, 2). An intriguing new direction of research, into the intersection of redox homeostasis and adult stem cell maintenance, raises questions about the effect of diabetes and hyperglycemia on stem/progenitor cells. Considering participation of bone marrow-derived multipotent stromal cells (BMSCs) in wound healing processes (3), the delay in tissue repair that we have found is synonymous with diabetes (4, 5) further asks whether diabetic BMSCs (dBMSCs) are aberrant or absent, and do not function in a regenerative environment. We aimed to explore whether diabetes and redox stresses critically affect BMSCs.

Metabolic changes and management of reactive oxygen species (ROS) are emerging as fundamental features that regulate cell identity across a range, from embryonic stem cells, to induced pluripotent stem cells, to bone-marrow-derived hematopoietic (HSCs) and BMSCs (6, 7). Studies on metabolic regulation of HSCs function and stemness are growing, but BMSC parallels are relatively scarce. Similar to their HSC neighbors (8, 9), BMSCs thrive and remain multipotent in the hypoxic environment of the bone marrow (BM) (10). BMSCs also retain their capacity to differentiate along osteogenic, adipogenic and chondrogenic lineages as they respond to non-native sites with oxidative imbalance, such as a hypoxic wound (11). As metabolic and redox dysregulation are such central features of diabetes, the mechanisms that enable BMSC metabolic modulation and those that preserve cell integrity in oxidative imbalance may be compromised.

A pathway that encompasses metabolic and cytoprotective roles, and is disrupted in diabetes is the Nuclear-factor-erythroid-related-factor-2 (Nrf2)/Kelch-like-erythroid-cell-derived-protein-1 (Keap1) pathway (12). Nrf2 is a transcription factor driving over 50 redox homeostasis-related genes, and nearly 200 genes influencing metabolism and repair (13). Keap1 functions as an intracellular ROS sensor, as oxidants and electrophiles modify its cysteine residues. Without ROS, Keap1 binds to Nrf2 and promotes Nrf2 proteasomal degradation. ROS accumulation disrupts the Keap1-Nrf2 interaction. Nrf2 binds with small Maf proteins to antioxidant response elements (AREs) in the regulatory regions of target genes. Key genes activated to respond to oxidative stress include *NAD(P)H-quinone-oxidoreductase-1 (NQO1*), *manganese-superoxide-dismutase (MnSOD), heme-oxygenase-1 (HO-1*), *glutamate-cysteine-ligase (GCL)* and *glutathione-S-transferases (GSTs*). A study found that human BMSCs in high ROS shift their metabolism to resemble differentiated cells, and increase expression of antioxidant enzymes, MnSOD and catalase (14). Nrf2 overexpression can reduce ROS-induced apoptosis and cytotoxicity in BMSCs through upregulation of MnSOD and HO-1 (15). In diabetes and chronic hyperglycemia, unusually high levels of superoxide leak from the mitochondrial electron transport chain during aerobic respiration (2). The rate of ROS scavenging cannot compensate, resulting in damaging oxidation of cellular components (16). Previously, we found that despite high ROS, diabetic skin has low Nrf2 activation and subsequently has low antioxidant expression to affect delayed wound healing outcomes (5). Whether Nrf2/Keap1-mediated redox regulation plays a role in dBMSCs, or affects their identity, that in turn can influence BMSC response during diabetic wound healing, is yet to be discovered. We postulate that to retain their multipotency and contribute to wound healing, BMSCs need to minimize ROS damage and preserve robust redox mechanisms.

Here, through comparison of wild type (WT) and dBMSCs, we identified dysregulated redox metabolism in dBMSCs leading to loss of multipotency, bias towards an adipogenic fate, and reduction of Nrf2-transcribed antioxidants. Using short-interfering-RNA (siRNA) against *Keap1*, we forced activation of the endogenous Nrf2 in dBMSCs to reprogram their metabolic and redox mechanisms, as well as restore multipotent cell behavior through Sox2 expression. Finally, we show that the Keap1 downregulation and Nrf2-activation-based rescue of dBMSCs enables them to participate in diabetic wound healing. We demonstrate the importance of intrinsic resistance mechanisms mediated by Nrf2/Keap1 in response to oxidative stress. Through the range of effects on redox homeostatic and metabolic maintenance mechanisms, the Nrf2/Keap1 pathway is critical in the maintenance of fate and function of adult BMSCs.

Research Design and Methods

Mice. C57BL/6J and BKS.Cg-Dock7$^{m+/+}$Lepr$^{db/J}$ (blood glucose ≥ 400 mg/dL) strains were from Jackson Laboratories. All protocols were approved by the IACUC at New York University School of Medicine.

BMSC culture and immunophenotyping. 6-8 weeks old mouse BM aspirates were cultured in Mesencult at 37°C/5%CO_2/5%O_2. After first media change, BMSCs were cultured in alpha-MEM supplemented with 15% fetal-bovine-serum, 1% non-essential amino acids. Low-glucose (LG) and high-glucose (HG) medium contained 1g/L and 4.5g/L d-glucose, respectively. BMSCs were detached using 3:2 accutase:trypsin-EDTA, resuspended in 1xPBS/5%FBS/0.1%NaN_3, Fc-blocked with anti-mouse-CD21/CD23, and stained with fluorophore-conjugated antibodies

against CD45, Ter119, Sca1, PDGFRα, CD29, CD44, CD73, CD90.2, CD105, CD34 or flk1 (Miltenyi), and analyzed on a BD-FACS-Calibur and FlowJo.

Single-cell colony-forming assay. BMSCs were plated into 96-well plates at 1 cell/3-wells. After 2 weeks, colonies stained with crystal violet were counted.

Adipogenic and osteogenic differentiation. For adipogenic induction, BMSCs were cultured in 0.5uM dexamethasone, 0.5mM IBMX, 50uM Indomethacin, with 1mM insulin for initial 4 days, and analyzed at 14days for Oil-Red-O-stained lipid droplets. For osteogenic induction, BMSCs were cultured in 100nM dexamethasone, 50μM ascorbate phosphate, 10mM β-glycerophosphate with 100ng/mL BMP2 every 2 days. After 14days, cells were analyzed for calcium deposits using alizarin red. Cells were photographed using a Zeiss Observer microscope.

Chondrogenic differentiation. $2.5x10^5$ cells were pelleted in 15mL tubes. Cell pellets were cultured in LG-α-MEM containing 1%FBS, 100nM dexamethasone, 50μg/mL ascorbic acid 2-P, 40μg/mL L-Proline, 1% ITS/supplement B-D, and 1mM sodium pyruvate with 10ng/mL TGFβ3 and 100ng/mL BMP2 added every 2 days. At 21days, pellets were fixed, embedded in agarose, processed into paraffin blocks, sectioned and stained for cartilage using Safranin-O.

siRNA transfection. BMSCs were seeded at 20,000cells/cm^2. Dilutions of siRNA and Lipofectamine2000 were mixed and incubated for 20minutes, before addition to cells. Media was changed 6hours later. Cells were harvested at 24, 48 or 72hours post-transfection for RNA and protein analyses.

Quantitative RT-PCR. From phenol-chloroform extraction, aqueous-phase RNA was precipitated with isopropanol and purified in spin columns of RNeasy kits (Qiagen). 500ng total RNA was reverse transcribed using the High-Capacity cDNA synthesis kit (ThermoFisher) and

quantified in real-time with SYBRgreen detector in a QuantStudio7-Flex (ThermoFisher), relative expressions were calculated by delta-delta-C_T method.

CM-H_2DCFDA assay. BMSCs were resuspended in HBSS and incubated in 10uM 5-(and-6)-chloromethyl-2′,7′-dichlorodihydrofluorescein diacetate **(**ThermoFisher) for 45minutes at 37°C/5%CO_2/5%O_2, then analyzed on a BD-FACS-Calibur.

Fluorogenic ROS-cytochemistry. CellROX (ThermoFisher) were added to BMSCs at 5μM for 30minutes at 37°C. Cells were counterstained with DAPI and photographed with an Olympus BX51 microscope.

8-OHdG measurement. 8-hydroxy-2'-deoxyguanosine (8-OHdG) was measured with Oxidative DNA Damage ELISA kit (Cell Biolaboratories). Wells of 96-well plates were coated with 100μL 8-OHdG-BSA/PBS-conjugate overnight at 4°C. After washes, plates were blocked with 200μL assay-diluent for 1hour at RT. 50μL samples and standards were incubated for 10minutes, followed by incubation with 50μL anti-8-OHdG antibody for 1hour. After washing, 100μL horseradish-peroxidase-coupled secondary antibody was incubated for 1hour. After several washes, 100μL of peroxidase-substrate solution was added. The reaction was stopped with 100μL stop solution after 5 minutes and measured at 450nm on the Synergy-H1 plate reader (BioTek), standardized to total DNA.

Immunocytochemistry. BMSCs were fixed for 10minutes using 4%paraformaldehyde/PBS, then permeabilized in 0.2%Tween/PBS and blocked 30minutes in 5% donkey serum (Jackson Immunoresearch). Nrf2 (ab92946, AbCam) and Keap1 (60027-1-Ig, Proteintech) antibodies were applied and detected with fluorophore-conjugated secondary antibodies. Cells were photographed on an Olympus BX51.

Protein lysates and Western Blot. Cells were lysed in 10mM HEPES (pH7.9), 10mM KCl, 0.1mM EDTA, 10mM DTT, 2x protease/phosphatase-inhibitor (Sigma-Aldrich). Following 15seconds vortexing, the lysate was centrifuged at 15,000*xg* for 20minutes to separate the cytoplasmic extract (supernatant) and nuclear extract (pellet). Cytoplasmic extract was removed into pre-chilled tubes. The nuclear extract pellet was resuspended in 20mM HEPES (pH7.9), 0.4M NaCl, 1mM EDTA, 25% glycerol, and 2x protease/phosphatase inhibitor mixture, and incubated for 10minutes. Nuclear lysate was separated by centrifugation at 15,000*xg* for 5minutes. Protein concentration was measured using Pierce 660nm Reagent (ThermoFisher) on a Nanodrop 2000. 20µg extracts were separated in 12% SDS-polyacrylamide gels and transferred to PVDF membranes (Biorad). The membrane was blocked for 2hours using a 5% non-fat-milk/Tris-buffered-saline/0.1% Tween (Pierce) and probed with Nrf2, Keap1, PCNA (2586, Cell Signaling), or β-actin (ab8229, AbCam) antibodies. HRP-conjugated secondary antibodies allowed protein detection on hyperfilm (Amersham) with ECL plus reagent.

MTT assay. 15µl premixed Dye of CellTiter 96®-Cell Proliferation Assay (Promega) was added to cells in 96-well plates for 4 hours at 37°C, to allow tetrazolium conversion into a formazan product. 100µl of Solubilization/Stop Solution per well solubilized the formazan product and plate read at 570nm.

Nrf2 ELISA. Nuclear and cytoplasmic extracts were prepared using the Active Motive™ Nuclear Extract Kit (No.40010), and concentrations measured using Pierce 660nm Reagent on Nanodrop 2000. Activated Nrf2 levels were determined using the TransAm™ Nrf2 ELISA kit (No.50296). 96-well plates that are coated with an ARE consensus sequence oligonucleotide, were blocked with DTT/herring-sperm-DNA buffer. 10µL samples and positive controls were added to wells, followed by Nrf2 antibody for 1hour incubation at RT. 100µL HRP-conjugated

secondary antibody was added per well for 1hour at RT. The ELISA was developed by sequentially adding 100µL each of Developing and Stop solution per well, and reading the plate at 450nm (reference 655nm). Nrf2 quantity was based on the positive control.

Keap1 ELISA. 100µL nuclear and cytoplasmic lysates were added to Keap1-antibody-coated plates (ABIN1980574) for 2hours at 37°C. After sample removal, 100µL Detection Reagent A was added per well for 1hour at 37°C. 100µL Detection Reagent B was added to each well for 30minutes at 37 °C. After washes, 90µL Substrate was added per well and incubated for 15-25minutes at 37°C to allow the liquid to turn blue. 50µL Stop Solution turned the liquid yellow and the plate was read at 450nm. Keap1 quantities were calculated based on a standard curve created with recombinant protein in the kit.

GSH/GSSG assay. Glutathione-S-transferase converts a luminogenic GSH (reduced) probe, luciferin-NT, to luciferin. BMSCs were lysed to release GSH and GSSG (oxidized). The lysis buffer for one set contained N-ethylmaleimide to block GSH, allowing luminescence from only GSH reduced from GSSG. Luminescence readings from the total glutathione and only GSSG were used to calculate the GSH/GSSG values.

Cellular metabolism assay. Agilent Seahorse Cell Mito Stress Kit was used. Briefly, 60,000 cells were seeded in Seahorse XF24 microplates, in low serum media to prevent changes in cell numbers. One hour before measurement of oxygen consumption rate (OCR) and extracellular acidification rate (ECAR), cells were washed with and switched to Seahorse Assay Medium (5mM or 25mM glucose by cell type, 2mM L-glutamine, no bicarbonate), and incubated without CO_2 to remove any traces. Data was collected at baseline and at intervals after sequential addition of inhibitors oligomycin (1µM), FCCP (2µM), and rotenone/antimycin A (0.5uM).

Following data collection, cells were counterstained and fixed. The plate was imaged using the Arrayscan VTI Acquisition Only protocol by collecting 9 tiles at 5x magnification and 2x2 pixel binning. Images were analyzed using the Morphology Explorer protocol (v4). Object identification was performed using 3D surface background subtraction, dynamic isodata thresholding of -0.5, and segmented by shape = 2 with object cleanup enabled. Objects touching the border of the image field were rejected from analysis. Between one and four fields/well were used to calculate the average number of cells per field area and used to extrapolate total cell counts in the entire well. Data was normalized to cell number.

Wounding and BMSC seeding. 10mm-full-thickness wounds were created on mice dorsum, then splinted open with 10mm-diameter silicone stents, that were secured by interrupted 4-0 nylon sutures (Ethicon). Photographs of stented wounds were analyzed for percent wound closure (non-healed wound/original wound), standardized to the internal stent diameter. Area-under-the-curve (AUC) was calculated using the trapezoidal rule (Graphpad Prism). BMSCs were seeded into wounds with a 20G needle. For histology, 10day wounds were harvested and fixed, processed into paraffin, sectioned and stained with H&E, or rabbit anti-mouse CD31 antibody (Cell Signaling), and scanned. Blood glucose was measured once a week to ensure diabetic mice retained $\geq$ 400 mg/dL glucose throughout the study period.

Statistical Analysis. Data are expressed as mean±standard deviation of at least 3 separate trials, each n=3. Students' t-tests and one-way-ANOVA were used. P-values less than 0.05 determined statistical significance.

Results

Diabetic BMSCs exhibit altered identity and compromised multipotency

To investigate whether diabetes induces changes in BMSCs, we compared immunophenotypes of BM aspirates between WT and db/db mice. Based on lack of expression of the hematopoietic markers, CD45 and Ter119, we identified 0.45% and 0.19% BMSCs in WT and db/db, respectively (Fig1A). We analyzed expression of Sca-1 and PDGFRα, as the combination enriches for BM-resident mesenchymal stem cells (17). $CD45^{-}Ter119^{-}Sca\text{-}1^{+}PDGFR\alpha^{+}$ BMSCs comprised 0.16% of the WT BM-aspirate, but only 0.072% of that of db/db mice (Fig1B). The 55% reduction in both $CD45^{-}Ter119^{-}$ and $Sca\text{-}1^{+}PDGFR\alpha^{+}CD45^{-}Ter119^{-}$ cells in db/db BM-aspirates compared to that of WT indicates a compromised dBMSC pool, including reduced number of mesenchymal stem cells. Analysis of passage 3 (P3) BM cells showed that the percentage of $CD45^{-}Ter119^{-}$ cells is consistently lower in db/db cultures (FigS1A). Of $CD45^{-}Ter119^{-}$ cells, the percentages of db/db $Sca\text{-}1^{+}$ and $PDGFR\alpha^{+}$ cells are 28.3% and 64% less than that of WT (FigS1B), respectively, while the db/db $Sca\text{-}1^{+}PDGFR\alpha^{+}$ fraction is only 8.47% of that of WT by P3 (Fig1C). Expression of other cell surface markers associated with BM stromal fraction revealed downregulation of CD29 and CD44 in P3 dBMSCs vs P3 WT-BMSCs, but upregulation of CD73 (FigS1C).

We then assessed whether the diabetic hyperglycemic conditions affect other multipotency characteristics. Single-cell colony forming assays revealed 12±4 colony forming units (CFUs) with dBMSCs, compared to 28.5±2.5 CFUs with WT-BMSCs at P1 (Fig1D). At P2, we observed 6.5±1.5 dBMSC CFUs and 30.5±1.5 WT-BMSC CFUs. At equivalent passages, dBMSCs had greater number of flat, polygonal cells (Fig1F, 55%) and lower number of spindle-shaped cells,

compared to WT-BMSCs (Fig1E). Flow cytometry forward scatter also revealed that dBMSCs have larger nuclei, compared to WT-BMSC nuclei (Fig1G). The larger morphology and nuclei are both indicative of differentiated cells. We then cultured both WT and db/db BMSCs in adipogenic, osteogenic or chrondrogenic media. dBMSCs could only successfully differentiate into adipocytes (Fig1H), indicating that diabetes precludes osteogenic and chondrogenic differentiation capacities. Our results reveal that in diabetic hyperglycemic conditions, phenotypic and behavioral changes in BMSCs reflect their altered identity.

Lack of Nrf2 activity in diabetic BMSCs corresponds with dysfunction in ROS management

To determine whether the lack of BMSC characteristics in diabetic mice corresponds with metabolic shifts, we assessed live ROS levels in dBMSCs, WT-BMSCs and stromal cells. ROS levels in dBMSCs are 3.34-fold higher than in WT-BMSCS (Fig2A-B). Between WT-BMSC and stromal cells, WT-BMSCs contain significantly lower ROS (Fig2C), suggesting dBMSCs are more similar to stromal cells than to WT-BMSCs. dBMSCs displayed high levels of non-reduced ROS in the cytoplasm (Fig2D). Small spindle-shaped dBMSCs showed nuclear and mitochondrial accumulation of ROS (Fig2E). The larger polygonal dBMSCs only show cytoplasmic ROS (Fig2D). ROS generation is associated with oxidative phosphorylation, which is observed in differentiated cells unlike glycolysis in primitive cell populations (7). To determine whether the high ROS in dBMSCs is associated with precocious oxidative phosphorylation and differentiation, we examined expression of key genes that identify this metabolic state. Gene expressions of CytC and ATPSynthaseF1, components of the electron transport chain during aerobic respiration, are upregulated in dBMSCs compared to WT-BMSCs (Fig2F). Interestingly, Cox4i, a subunit of cytochrome oxidase that transfers electrons to oxygen

in the final steps of the electron transport chain and prevents buildup of H_2O_2, is downregulated in dBMSCs, compared to WT-BMSCs (Fig2F). For a functional readout, we analyzed bioenergetic profiles of WT and dBMSCs, and found consistently higher glycolytic indices in similar numbers of dBMSCs, than WT-BMSCs (Fig2G, FigS2A). Mitochondrial respiration rates demonstrate that dBMSCs have significantly higher oxidative phosphorylation indices than WT-BMSCs (Fig2H, FigS2B). However, dBMSCs also demonstrate sharp depletion of mitochondrial reserve capacity with a second addition of FCCP, which maximizes respiration steadily in WT-BMSCs (Max 2, Fig2H). Combination of glycolytic and mitochondrial respiration profiles indicates that dBMSCs do not display the glycolytic profile seen in WT-BMSCs and characteristic of progenitor cells. Of interest, increasing passages of WT-BMSCs demonstrate a shift away from a glycolytic profile as well, towards that of dBMSCs (Fig 2I).

As the Nrf2/Keap1 pathway would typically manage ROS burdens, we analyzed key components. Protein expression demonstrated that Nrf2 is less abundant in nuclei of dBMSCs, compared to WT-BMSCs (Fig2J). Concurrently, Keap1 is strongly upregulated in dBMSC cytoplasm, compared to WT-BMSCs (Fig2K). Immunocytochemistry showed significant upregulation in cytoplasmic Keap1 in dBMSCs compared to that of WT-BMSCs (Fig2L). *NQO1* and *MnSOD* gene expression showed significant downregulation in dBMSCs (Fig2M). Due to disruption of the Nrf2/Keap1 antioxidant pathway in diabetes, dBMSCs show reduced ability to manage ROS, concomitant with a conspicuous shift away from typical glycolytic metabolism of multipotent cells and towards energetic oxidative phosphorylation seen in differentiated cells. Our results thus far indicate that the uncoupling of ROS accumulation and Nrf2 release from Keap1, and consequently, downregulation of intrinsic Nrf2-mediated redox regulatory mechanisms in dBMSCs propels differentiation at the cost of multipotency.

Silencing *Keap1* upregulates antioxidant mechanisms in dBMSCs

Based on anomalous levels of Nrf2 and Keap1 in dBMSCs, we analyzed *Keap1* gene expression and found 1.65±0.1-fold increase in dBMSCs compared to WT-BMSCs (Fig3A). To restore nuclear Nrf2 activity, we silenced *Keap1* in dBMSCs using siRNA, while cells were still cultured in hyperglycemic conditions. We detected 65±7.9% *Keap1* knockdown compared to untreated dBMSCs and 41.5±1.3% knockdown compared to WT-BMSCs (Fig3A). With si*Keap1* in WT-BMSCs, cytoplasmic Keap1 protein sharply decreased in contrast to untreated cells (Fig3B,C). In dBMSCs, *Keap1* silencing results in remarkable reduction in Keap1 protein as well (Fig3B, C). *Keap1* knockdown in WT-BMSCs and dBMSCs resulted in significant upregulation of nuclear Nrf2, compared to untreated cells (Fig3B, D). Immunocytochemistry revealed that Nrf2 is present in the nucleus in si*Keap1*-dBMSCs, along with a conspicuous lack of Keap1 in the cytoplasm (Fig3E). Next, we investigated whether Nrf2 upregulation affects redox homeostasis of dBMSCs. ROS levels of si*Keap1*-dBMSCs diminished significantly, compared to untreated dBMSCs (Fig3F). *Keap1* inhibition in dBMSCs increased $CD45^{-}/Ter119^{-}$/Sca-1+/PDGFRα+ cells to 1.4% (Fig3G), a nearly five-fold increase from their original numbers (Fig1C). We then quantified 8-OHdG, a bio-marker of oxidative stress, between WT and si*Keap1*-dBMSCs. In dBMSCs, silencing *Keap1* results in a significant decrease in 8-OHdG concentrations to near WT levels (Fig3H). Fluorogenic indicators also confirmed the diminished levels of cytoplasmic ROS in siKeap1-dBMSCs, with 32.22±11.24% of siKeap1-dBMSCs containing ROS in stark contrast to 86.11±15.26% of dBMSCs (FigS2A-B).

To assess Nrf2 activity, we examined the expression of key transcripts following *Keap1* silencing. In comparison to untreated dBMSCS, gene expressions of *NQO1* and *MnSOD* are significantly upregulated (Fig3I-J). *Nox4*, known for its protective functions in redox

management (18), was upregulated (Fig3K). Gene expression of other Nrf2-transcribed antioxidant molecules, *HO-1*, glutathione-S-reductase (*GSR*), glutathione-peroxidase-1 (*Gpx*1), *GST*μ1, *GST*α3 followed the significant upregulation trend (Fig S3). To further evaluate the metabolic effects of upregulating Nrf2 levels, we assessed the GSH/GSSG ratio, an indicator of cellular redox status that is regulated by Nrf2-targets (19). Silencing *Keap1* raises the GSH/GSSG ratio in dBMSCs compared to untreated cells ($p<0.005$), and similar to GSH/GSSG in WT-BMSCs (Fig3L). These data suggest that restoring expression of the major regulator Nrf2 can resolve the diabetes-induced aberrant intracellular redox homeostasis and metabolic routes in dBMSCs.

Nrf2 activity rescues multipotent cell traits in dBMSCs

Having successfully rescued the diabetes-induced disruptions in the Nrf2/Keap1 pathway in dBMSCs, we now assessed the role of Nrf2/Keap1 in cell identity in high ROS. As Nrf2 upregulation increased percentage of immature dBMSCs, we analyzed their differentiation potential. Quantity of lipids present in native dBMSCs resembles that of purposefully adipogenic-differentiated si*Keap1*-treated ones (Fig4Ai). This indicates dBMSCs exhibit precocious adipogenic differentiation. Unlike the absence of red calcium deposits in native dBMSCs, the *Keap1*-silenced cells in osteogenic media have remarkable staining (Fig4Aii). In contrast to native dBMSCS, si*Keap1*-treated cells show the onset of chondrogenic differentiation (Fig4Aiii). We further analyzed expression of genes associated with each lineage among WT-BMSCs, dBMSCs, and si*Keap1*-dBMSCs. At basal stages, adipogenesis associated gene, adipocyte-protein-2 (*aP2*), is similar between WT and dBMSCs (Fig4B), while peroxisome-proliferator-activated-receptor-γ (*PPARγ*) is upregulated in dBMSCs relative to WT-BMSCs (Fig4C). At 3 days into adipogenic induction, both *aP2* and *PPARγ* are significantly

overexpressed in dBMSCs, compared to WT-BMSCs (Figure4B,C). si*Keap1*-dBMSCs significantly reduce both genes. Then, we analyzed osteogenic genes – bone-morphogenetic-protein-2 (*BMP2*), osterix (*Osx*) and runt-related-transcription-factor-2 (*RUNX2*). At day0, *BMP2* expression in dBMSCs is remarkably downregulated, compared to WT-BMSCs (Fig4D). At day3 of osteogenic induction, while WT-BMSCs showed downregulation of *BMP2*, dBMSCs show abnormal upregulation. si*Keap1*-dBMSCs reduce *BMP2* expression, similar to WT-BMSCs. Compared to WT-BMSCs, the irregular temporal pattern of gene expression in dBMSCs is apparent with *Osx* and *RUNX2* as well, but is restored with si*Keap1* (Fig4E,F). For chondrogenic induction, dBMSCs showed downregulation of collagen-type-2-alpha-I (*Col2aI*) and aggrecan (*ACAN*) with respect to WT-BMSCs, but with si*Keap1*, gene expression followed the WT-BMSC pattern (Fig4G, H). Our data indicates that activation of Nrf2 is necessary for multilineage differentiation, and this capacity can be restored in dBMSCs.

To evaluate the extent of restoration of typical multipotent cell features in *Keap*1-silenced dBMSCs, we used analyzed BMSC migration capacity towards SDF1, as BMSCs express the CXC-chemokine-receptor-4 (CXCR4) (20). dBMSCs exhibit reduced migratory capacity, compared to WT-BMSCs (Fig4I). *Keap1* silencing not only rescues this behavior but boosts migration capacity over that of WT-BMSCs (Fig4I). We explored gene expression of *CycD1* and *CycD2*, which allow cell cycle progression, and found significantly downregulated expression in dBMSCs, compared to WT-BMSCs. *Keap1* inhibition in dBMSCs resulted in statistically significant upregulation of both *CycD1* and *CycD2*, compared to untreated dBMSCs (Fig4J). Next, we measured the proliferation of WT-BMSCs, dBMSCs and si*Keap1*-dBMSCs. At all time points following transfection with si*Keap1*, si*Keap1*-dBMSCs had nearly twice the quantity of cells, compared to untreated ones (Fig4K). Nrf2 activity restores not only multipotency of

dBMSCs, but their behavioral aspects as well. Our results indicate that BMSCs require functional Nrf2/Keap1 signaling to maintain cell identity in unusual redox conditions, as in diabetes.

Nrf2 activity in BMSCs is coupled to Sox2 expression

Searching for candidates that further examine the Nrf2-initiated mechanisms in retaining BMSC multipotency, we came across Sox2 that regulates self-renewal and stemness of osteo-adipo lineage cells (21). We analyzed whether *Sox2* expression is affected by modulation in Nrf2 activity. WT-BMSCs and dBMSCs did not show differential expression (Fig5A). However, a time course analysis following *Keap1* inhibition showed that dBMSCs significantly upregulated *Sox2* expression, particularly at 48 and 72 hours, in relation to native dBMSCs (Fig5B). Additionally, analysis of gene expression of *Yes-associated protein 1* (*YAP1*), a direct downstream target and effector of Sox2 (21), showed similar upregulation at 48 and 72 hours post-si*Keap1* transfection. To analyze functional consequence of the transient upregulation of *Sox2* brought induced by Nrf2, we analyzed differentiation potential of si*Keap1*-dBMSCs with and without Sox2. We knocked down *Nrf2* using siRNA and/or *Sox2* using shRNA in WT-BMSCs. We also knocked down *Keap1* and *Sox2* in dBMSCs, in si*Keap1*-dBMSCs. Following 2 weeks in osteogenic media, si*Nrf2*-WT-BMSCs showed poor alizarin red staining, indicating poor osteogenesis (Fig5C). WT-BMSCs with both *Nrf2* and *Sox2* knockdown displayed similar failure. In dBMSCs, the simultaneous knockdown of *Sox2* and *Keap1* negated the osteogenic capacity induced by only *Keap1* inhibition. Our results suggest that Sox2 and YAP are necessary to impart the BMSC multipotency that is regulated by Nrf2 and compromised in diabetes.

Lack of Nrf2/Keap1 signaling in diabetic BMSCs limits their role in tissue regeneration

As BMSCs orchestrate repair/regeneration in a wound setting (3), we assayed the impact of Nrf2/Keap1 activity on this capacity using cultured BMSCs in a previously established wound model (22). We seeded the wound with BMSCs and monitored time to closure as a readout of BMSC function during repair (Fig6A). The addition of any BMSCs provided an advantage to diabetic wound closure and healing. Addition of siNS-dBMSCs accelerated healing time to 25.5±2.12 days, compared to untreated diabetic wounds at 31.25±1.5 days (Fig6B-D). Wounds with WT-BMSCs and si*Keap1*-dBMSCs demonstrated the most significant reduction in wound healing time to 22±2.4 days and 20.75±2.36 days, respectively (Fig6B,C). These data indicate that Nrf2 induction by si*Keap1* enables dBMSCs to successfully coordinate tissue repair, like WT-BMSCs. For diabetic wounds with si*Keap1*-BMSCs, the decrease in pathological wound burden correlated with the significant decrease in time to closure (Fig6C-D, FigS4A). Wound healing rates further highlight the impact of seeding si*Keap1*-dBMSCs to diabetic wounds in comparison to untreated wounds (FigS4B). As BMSCs exert their repair role in the granulation tissue, we analyzed tissue sections of the wound bed. WT and si*Keap1*-dBMSCs promote larger areas of granulation tissue in the healing edges compared to siNS-dBMSC-treated diabetic wounds (Fig6E). In addition, WT and si*Keap1*-dBMSCs significantly increased CD31+ neovascularization in the granulation tissue, compared to siNS cells (Fig6F), a feature that BMSCs typically contribute to during repair (23). Isotype controls for the primary antibodies failed to show any immunoreactivity (data not shown). Our data demonstrate that restoration of the Nrf2/Keap1 signaling axis in dBMSCs normalizes their capacity to facilitate tissue regeneration, even in an environment presenting extracellular redox stresses.

Discussion

Knowledge of molecular regulators and their deficits in diabetes is critical to enable specificity and efficacy in therapeutic approaches. We previously showed that lack of tissue repair in the extreme redox imbalance of diabetic wound healing is due to dysregulated Nrf2/Keap1 signaling (5). As BMSCs contribute to wounds with oxidative stress to limit tissue damage and promote tissue re-growth (3, 24), we explored the effect of diabetes on BMSCs. We established that Nrf2-mediated transcription in BMSCs influences cellular metabolism through redox management to affect differentiation status.

We found diabetes induced unusually high ROS accumulation in dBMSCs, similar to reported diabetic bone marrow-derived cells (25), along with significantly increased Keap1 expression, downregulation of Nrf2 and downstream redox enzymes. Normalization of Nrf2/Keap1 levels produced upregulation of antioxidant enzymes, diminishing ROS levels, and restoration of metabolism in dBMSCs. 8-OHdG decreased and GSH/GSSG increased to WT levels, possibly due to Nrf2-regulated DNA repair enzymes (26) and transcription of GCL-catalytic subunits, respectively (13). Low GSH in dBMSCs is likely exacerbated by the polyol pathway in diabetes, due to lack of NADPH also regulated by Nrf2/Keap1 (2, 27). We show that Nrf2/Keap1 is a major determinant of low ROS, a known requirement in glial progenitors and HSCs also (28, 29). This redox management is conserved across vertebrate and invertebrate HSCs (30, 31), and intestinal stem cells (32). Activation of the Nrf2/Keap1 pathway mitigates oxidative stress in adult mouse BMSCs in their native state and prevents multifaceted metabolic deficiencies, but is severely compromised with the extrinsic environment in diabetes.

Lack of multipotency in dBMSCs corresponded to phenotypic and morphological features of differentiated cells, and expression of oxidative phosphorylation genes. A preference for glycolysis in wild type BMSCs is not surprising given the hypoxic nature of bone marrow. However, dBMSCs exhibited metabolic profiles associated with differentiated cells as well, such as high energy-producing oxidative phosphorylation. The high ATP-linked respiration and higher basal respiration in dBMSCs, together with proton leak and less Cox4i, with higher ROS may explain this observation. Premature differentiation in diabetes possibly limits the pool of self-renewing BMSCs. Forced downregulation of Keap1 and thus Nrf2 activation, and subsequent Sox2 expression, reverted the adipogenic differentiation bias in dBMSCs and enabled them to respond to distinct lineage induction cues in culture. Sox2 is a sensitive transcription factor, well recognized for its role in maintenance of multipotency in osteoblasts (21), and proliferation potential (33). Similar to our findings of the deficiencies in dBMSCs, Nrf2 and Sox2 are required for proliferation in glioma stem cells (34). A well-tuned homeostatic balance of Keap1 and Nrf2 is obviously vital, as loss of Keap1 has been shown to lead to hyperproliferation, Nrf2 is known to regulate SIRT1 which post-translationally regulates Sox2 in human bone marrow derived mesenchymal stem cells (35), Metabolic changes in pluripotent and cancer cells have been shown to alter their cell differentiation status (36), not unlike the changes in diabetes. Mitochondrial ROS accumulation is sufficient to trigger adipocyte differentiation in human BMSCs (37) to resemble dBMSCs. ROS in fact primes Drosophila HSCs for a specific lineage (30). Similar to our approach, the authors prevent Drosophila HSC differentiation by neutralizing ROS. Even in a whole organ, such as the mouse liver, Nrf2 negatively regulates lipid biosynthetic mechanisms (38). Our results would then indicate that Nrf2/Keap1 signaling is required to preserve the multipotency of BMSCs in cooperation with

Sox2. In diabetes, long term hyperglycemia and persistent downregulation of Nrf2 signaling via Keap1 is a switch for adipogenic differentiation.

Improvement in time to closure of diabetic wounds when seeded with Nrf2-activated dBMSCs illustrated the link between redox and multipotency status of BMSCs, and their ability to coordinate successful healing. Muted Nrf2/Keap1 signaling in dBMSCs negatively affected migratory capacity and proliferation in culture, to possibly affect mobilization of BMSCs into injury sites, and insufficient healing events in diabetic tissues. A supporting study found that neovascularization was impaired in diabetes models due to defective adipose-derived MSCs (24). We demonstrate that metabolic shifts that characterize diseases like diabetes trickle down to the level of stem/progenitor cells, crippling their populations, identity, behavior to limit regenerative ability. Existing literature describes the detrimental effects of diabetes and hyperglycemia, such as depletion of endothelial precursor cells, as irreversible through glycemic control (39). Focusing on the mechanisms that modulate metabolism offers options to rescue these detrimental changes at a cellular level at least. The hyperglycemia induced ROS accumulation can be restored at a local tissue (5) and cellular level.

Our study strongly indicates that co-induction of the redox and metabolism modulatory roles of the Nrf2/Keap1 pathway governs the identity of mouse BMSCs. We showed that diabetes diminishes properties and alters cell fates of BMSCs by unhinging the endogenous Nrf2/Keap1-mediated antioxidant mechanisms that are at the core of ROS management (Fig 7). The lack of Nrf2 signaling reprograms metabolism in diabetic BMSCs to add to ROS mismanagement and indicates a need for low ROS for maintenance. In Drosophila, constitutive Nrf2 or CncC activation limits proliferation of intestinal stem cells (ISCs) by keeping ROS in check (32). In response to injury and regenerative need, Keap1 represses CncC to induce proliferation. Though

mouse BMSCs require Nrf2 activation to proliferate in very obvious discrepancy with Drosophila ISCs, Nrf2 activation maintains the stem cell pool in intestinal stem cells and our BMSC model. In-depth understanding of the metabolic changes in BMSC regulation will allow us to address diabetic complications and design rescues for desired outcomes. In a departure from traditional signaling and growth factors in cell lineage, we show evidence that the Nrf2/Keap1 pathway has a much broader cytoprotective role in BMSCs than appreciated, encompassing redox homeostasis and metabolic modulation to determine cell identity and maintenance.

Acknowledgements

We are very grateful to Camille Kim, Rita Abigail Sartor, Bukhtawar Waqas for assistance with bone marrow harvests. We would like to thank Dr. Alka Mansukhani and Dr. Narendra Verma for sharing the shSox2 vector components. We would like to thank Dr. Morris Birnbaum for critical reading of the manuscript. This study was partially supported by American Diabetes Association Pathway Award 1-16-ACE-08 to D.C., and NYU Kimmel Stem Cell training grant to M.S. We are grateful to the Cytometry and Cell Sorting Core, the Experimental Pathology Core, Microscopy Core, and High Throughput Biology Core at NYU Langone Medical Center, supported in part by the Laura and Isaac Perlmutter Cancer Center Support Grant NIH/NCI P30CA016087, the NIH S10 OD010584-01A1 and S10 OD018338-01grants, NYSTEM Contract C026719, and the Helen L. and Martin S. Kimmel Center for Stem Cell Biology.

Author Contributions

P.S.R. designed and performed experiments, analyzed data, wrote and reviewed manuscript, and has no conflicts of interest; M.A.S. designed and performed experiments and analyzed data, and

has no conflicts of interest; R.L.K., S.H., A.M., M.K. assisted with experiments, and have no conflicts of interest; D.C reviewed manuscript and has no conflicts of interest. P.S.R and D.J.C. are the guarantors of this work and, as such, had full access to all the data in the study and take responsibility for the integrity of the data and the accuracy of the data analysis.

REFERENCES

1. Houstis N, Rosen ED,Lander ES, Reactive oxygen species have a causal role in multiple forms of insulin resistance. Nature, 2006. 440(7086): p. 944-948.
2. Giacco F,Brownlee M, Oxidative stress and diabetic complications. Circulation research, 2010. 107(9): p. 1058-1070.
3. Malhotra S, Hu MS, Marshall CD, Leavitt T, Cheung ATM, Gonzalez JG, Kaur H, Lorenz HP,Longaker MT, Mesenchymal Stromal Cells as Cell-Based Therapeutics for Wound Healing. Stem cells international, 2016. 2016: p. 4157934.
4. Ceradini DJ, Yao D, Grogan RH, Callaghan MJ, Edelstein D, Brownlee M,Gurtner GC, Decreasing intracellular superoxide corrects defective ischemia-induced new vessel formation in diabetic mice. The Journal of biological chemistry, 2008. 283(16): p. 10930-10938.
5. Soares MA, Cohen OD, Low YC, Sartor RA, Ellison T, Anil U, Anzai L, Chang JB, Saadeh PB, Rabbani PS,Ceradini DJ, Restoration of Nrf2 signaling normalizes the regenerative niche. Diabetes, 2015.
6. Wanet A, Arnould T, Najimi M,Renard P, Connecting Mitochondria, Metabolism, and Stem Cell Fate. Stem cells and development, 2015. 24(17): p. 1957-1971.
7. Ito K,Suda T, Metabolic requirements for the maintenance of self-renewing stem cells. Nature reviews. Molecular cell biology, 2014. 15(4): p. 243-256.
8. Cipolleschi MG, Dello Sbarba P,Olivotto M, The role of hypoxia in the maintenance of hematopoietic stem cells. Blood, 1993. 82(7): p. 2031-2037.
9. Hermitte F, Brunet de la Grange P, Belloc F, Praloran V,Ivanovic Z, Very low O2 concentration (0.1%) favors G0 return of dividing CD34+ cells. Stem cells, 2006. 24(1): p. 65-73.
10. Fehrer C, Brunauer R, Laschober G, Unterluggauer H, Reitinger S, Kloss F, Gully C, Gassner R,Lepperdinger G, Reduced oxygen tension attenuates differentiation capacity of human mesenchymal stem cells and prolongs their lifespan. Aging cell, 2007. 6(6): p. 745-757.
11. Rochefort GY, Delorme B, Lopez A, Herault O, Bonnet P, Charbord P, Eder V,Domenech J, Multipotential mesenchymal stem cells are mobilized into peripheral blood by hypoxia. Stem cells, 2006. 24(10): p. 2202-2208.
12. Kensler TW, Wakabayashi N,Biswal S, Cell survival responses to environmental stresses via the Keap1-Nrf2-ARE pathway. Annual review of pharmacology and toxicology, 2007. 47: p. 89-116.
13. Hayes JD,Dinkova-Kostova AT, The Nrf2 regulatory network provides an interface between redox and intermediary metabolism. Trends in biochemical sciences, 2014. 39(4): p. 199-218.
14. Chen CT, Shih YR, Kuo TK, Lee OK,Wei YH, Coordinated changes of mitochondrial biogenesis and antioxidant enzymes during osteogenic differentiation of human mesenchymal stem cells. Stem cells, 2008. 26(4): p. 960-968.
15. Mohammadzadeh M, Halabian R, Gharehbaghian A, Amirizadeh N, Jahanian-Najafabadi A, Roushandeh AM,Roudkenar MH, Nrf-2 overexpression in mesenchymal stem cells reduces oxidative stress-induced apoptosis and cytotoxicity. Cell stress & chaperones, 2012. 17(5): p. 553-565.

16. Evans JL, Goldfine ID, Maddux BA,Grodsky GM, Are oxidative stress-activated signaling pathways mediators of insulin resistance and beta-cell dysfunction? Diabetes, 2003. 52(1): p. 1-8.
17. Houlihan DD, Mabuchi Y, Morikawa S, Niibe K, Araki D, Suzuki S, Okano H,Matsuzaki Y, Isolation of mouse mesenchymal stem cells on the basis of expression of Sca-1 and PDGFR-alpha. Nature protocols, 2012. 7(12): p. 2103-2111.
18. Kovac S, Angelova PR, Holmstrom KM, Zhang Y, Dinkova-Kostova AT,Abramov AY, Nrf2 regulates ROS production by mitochondria and NADPH oxidase. Biochim Biophys Acta, 2015. 1850(4): p. 794-801.
19. Mitsuishi Y, Taguchi K, Kawatani Y, Shibata T, Nukiwa T, Aburatani H, Yamamoto M,Motohashi H, Nrf2 redirects glucose and glutamine into anabolic pathways in metabolic reprogramming. Cancer cell, 2012. 22(1): p. 66-79.
20. Son BR, Marquez-Curtis LA, Kucia M, Wysoczynski M, Turner AR, Ratajczak J, Ratajczak MZ,Janowska-Wieczorek A, Migration of bone marrow and cord blood mesenchymal stem cells in vitro is regulated by stromal-derived factor-1-CXCR4 and hepatocyte growth factor-c-met axes and involves matrix metalloproteinases. Stem cells, 2006. 24(5): p. 1254-1264.
21. Seo E, Basu-Roy U, Gunaratne PH, Coarfa C, Lim DS, Basilico C,Mansukhani A, SOX2 regulates YAP1 to maintain stemness and determine cell fate in the osteo-adipo lineage. Cell Rep, 2013. 3(6): p. 2075-2087.
22. Galiano RD, Michaels Jt, Dobryansky M, Levine JP,Gurtner GC, Quantitative and reproducible murine model of excisional wound healing. Wound repair and regeneration : official publication of the Wound Healing Society [and] the European Tissue Repair Society, 2004. 12(4): p. 485-492.
23. Chen L, Tredget EE, Wu PY,Wu Y, Paracrine factors of mesenchymal stem cells recruit macrophages and endothelial lineage cells and enhance wound healing. PloS one, 2008. 3(4): p. e1886.
24. Rennert RC, Sorkin M, Januszyk M, Duscher D, Kosaraju R, Chung MT, Lennon J, Radiya-Dixit A, Raghvendra S, Maan ZN, Hu MS, Rajadas J, Rodrigues M,Gurtner GC, Diabetes impairs the angiogenic potential of adipose-derived stem cells by selectively depleting cellular subpopulations. Stem cell research & therapy, 2014. 5(3): p. 79.
25. Yan J, Tie G, Wang S, Messina KE, DiDato S, Guo S,Messina LM, Type 2 diabetes restricts multipotency of mesenchymal stem cells and impairs their capacity to augment postischemic neovascularization in db/db mice. Journal of the American Heart Association, 2012. 1(6): p. e002238.
26. Singh B, Chatterjee A, Ronghe AM, Bhat NK,Bhat HK, Antioxidant-mediated up-regulation of OGG1 via NRF2 induction is associated with inhibition of oxidative DNA damage in estrogen-induced breast cancer. BMC cancer, 2013. 13: p. 253.
27. Wu KC, Cui JY,Klaassen CD, Beneficial role of Nrf2 in regulating NADPH generation and consumption. Toxicol Sci, 2011. 123(2): p. 590-600.
28. Smith J, Ladi E, Mayer-Proschel M,Noble M, Redox state is a central modulator of the balance between self-renewal and differentiation in a dividing glial precursor cell. Proceedings of the National Academy of Sciences of the United States of America, 2000. 97(18): p. 10032-10037.

29. Jang YY,Sharkis SJ, A low level of reactive oxygen species selects for primitive hematopoietic stem cells that may reside in the low-oxygenic niche. Blood, 2007. 110(8): p. 3056-3063.
30. Owusu-Ansah E,Banerjee U, Reactive oxygen species prime Drosophila haematopoietic progenitors for differentiation. Nature, 2009. 461(7263): p. 537-541.
31. Tsai JJ, Dudakov JA, Takahashi K, Shieh JH, Velardi E, Holland AM, Singer NV, West ML, Smith OM, Young LF, Shono Y, Ghosh A, Hanash AM, Tran HT, Moore MA,van den Brink MR, Nrf2 regulates haematopoietic stem cell function. Nature cell biology, 2013. 15(3): p. 309-316.
32. Hochmuth CE, Biteau B, Bohmann D,Jasper H, Redox regulation by Keap1 and Nrf2 controls intestinal stem cell proliferation in Drosophila. Cell stem cell, 2011. 8(2): p. 188-199.
33. Go MJ, Takenaka C,Ohgushi H, Forced expression of Sox2 or Nanog in human bone marrow derived mesenchymal stem cells maintains their expansion and differentiation capabilities. Exp Cell Res, 2008. 314(5): p. 1147-1154.
34. Zhu J, Wang H, Sun Q, Ji X, Zhu L, Cong Z, Zhou Y, Liu H,Zhou M, Nrf2 is required to maintain the self-renewal of glioma stem cells. BMC Cancer, 2013. 13: p. 380.
35. Yoon DS, Choi Y, Jang Y, Lee M, Choi WJ, Kim SH,Lee JW, SIRT1 directly regulates SOX2 to maintain self-renewal and multipotency in bone marrow-derived mesenchymal stem cells. Stem Cells, 2014. 32(12): p. 3219-3231.
36. Pereira SL, Rodrigues AS, Sousa MI, Correia M, Perestrelo T,Ramalho-Santos J, From gametogenesis and stem cells to cancer: common metabolic themes. Hum Reprod Update, 2014. 20(6): p. 924-943.
37. Tormos KV, Anso E, Hamanaka RB, Eisenbart J, Joseph J, Kalyanaraman B,Chandel NS, Mitochondrial complex III ROS regulate adipocyte differentiation. Cell Metab, 2011. 14(4): p. 537-544.
38. Yates MS, Tran QT, Dolan PM, Osburn WO, Shin S, McCulloch CC, Silkworth JB, Taguchi K, Yamamoto M, Williams CR, Liby KT, Sporn MB, Sutter TR,Kensler TW, Genetic versus chemoprotective activation of Nrf2 signaling: overlapping yet distinct gene expression profiles between Keap1 knockout and triterpenoid-treated mice. Carcinogenesis, 2009. 30(6): p. 1024-1031.
39. Januszyk M, Sorkin M, Glotzbach JP, Vial IN, Maan ZN, Rennert RC, Duscher D, Thangarajah H, Longaker MT, Butte AJ,Gurtner GC, Diabetes irreversibly depletes bone marrow-derived mesenchymal progenitor cell subpopulations. Diabetes, 2014. 63(9): p. 3047-3056.

Figure 1. Diabetic BMSCs demonstrate reduced multipotent cell characteristics.

A) Non-hematopoietic fractions of bone marrow aspirates between WT and db/db mice. B) Phenotypic comparison of $CD45^{-}/Ter119^{-}/PDGFR\alpha^{+}/Sca\text{-}1^{+}$ BMSCs in WT and db/db bone-marrow aspirates, using cell surface markers. C) $CD45^{-}/Ter119^{-}/PDGFR\alpha^{+}/Sca\text{-}1^{+}$ BMSCs in passage 3 cell culture. D) Single cell-based colony forming assay. E-F) Morphology of WT and dBMSCs in culture. G) Comparison of nuclei size between WT and dBMSCs. H) Stained WT and dBMSCs after 14 days in differentiation media as indicated. Data represented as mean ± sd, n≥3. See also Figure S1.

Figure 2. Nrf2/Keap1 pathway affected in altered diabetic BMSCs

A) Detection of intracellular ROS using CM-H_2DCFDA. ROS induces deacetylation of cell-permeant CM-H_2DCFDA to fluorescent DCF (Ex/em 492–495/517–527 nm) that is trapped. B) Quantification of intracellular ROS. C) Comparison of ROS levels between WT-BMSCs and stromal cells using CM-H_2DCFDA. D-E) Fluorogenic detection of ROS in cytoplasm (red), and nuclei and mitochondria (green). F) Gene expression of oxidative phosphorylation genes. G) Glycolytic indices, derived from Seahorse Mito Stress analysis. (H) Mitochondrial respiratory indices, derived from Seahorse Mito Stress analysis. I) Energy map of WT and dBMSCs, comparison between passages 3 and 6. J-K) ELISA of nuclear Nrf2 and cytoplasmic Keap1 using lysates of WT and dBMSCs. L) Immunofluorescence of Nrf2 and Keap1 proteins in WT and dBMSCs. M) Relative expression of Nrf2 target genes in WT vs dBMSCs. Data represented as mean ± sd. *, $p<0.05$, n≥3. See also Figure S2.

Figure 3. Knockdown of *Keap1* restores Nrf2-mediated antioxidant and metabolic mechanisms in dBMSCs

A) Relative expression of *Keap1* following silencing, 24 hours post-transfection. NS served as a negative control for transfection. B) Immunoblot of nuclear and cytoplasmic lysates of untreated and silenced WT and dBMSCs, 48 hours post-transfection. C-D) Relative protein expression of Nrf2 and Keap1 in cells as indicated. E) Immunofluorescence of Nrf2 and Keap1 in dBMSCs transfected with siNS or si*Keap1*. F) Flow cytometric analysis of intracellular ROS of indicated cells after *Keap1* silencing, using CM-H_2DCFDA. G) Percentage of PDGFRα^+/Sca-1^+ dBMSCs following si*Keap1* application. H) Quantification of 8-OHdG adducts, an indicator of ROS-mediated DNA damage. I-K) QRT-PCR of Nrf2 transcribed genes as indicated. L) Total glutathione in cells. Data represented as mean ± sd. *, $p<0.05$; **, $p<0.01$, $n\geq3$. See also Figure S3, S4.

Figure 4. Nrf2 activation restores multipotency in diabetic BMSCs

A) Stained db/db and si*Keap1*-dBMSCs at P3 and 14 days in differentiation media as indicated. B-C) Relative expression of adipogenic genes. D-F) Relative expression of osteogenic genes. G-H) Relative expression of chondrogenic genes. I) Transwell migration assay using WT or dBMSCs as indicated. J) Relative expression of cell cycle regulators. K) Proliferation in cells using MTT assay. Data represented as mean ± sd. *, $p<0.05$; **, $p<0.01$, $n\geq3$.

Figure 5. BMSC multipotency dependent on restoration of Sox2 expression

A) Relative expression of Sox2. B) Time course of relative expression of Sox2 and YAP following *Keap1* knockdown. *, $p<0.05$ in comparison to untreated dBMSCs. C) Alizarin red staining of BMSCs as indicated, after 2 weeks in osteogenic media.

Figure 6. si*Keap1* transfected dBMSCs reconstitute role in repair

A) BMSCs from WT or db/db mice were cultured and prepared 24 hours prior, with our without transfection with si*Keap1*. 5,000,000 cells in 300uL were injected into the cutaneous wound bed and immediate periphery, 24 hours post-excision. 100µL was seeded into the wound bed and the remaining 200µL was seeded in 50µL aliquots in the immediate wound periphery. B) Photographs of excisional wounds inoculated with BMSCs as indicated. C) Mean time to closure of cutaneous wounds. D) Photometric quantification of wound area. E) H&E stains of tissue sections of 10d wounds. Wound is to the left of image. Dashed black line, wound edge epidermis. E) CD31 immunohistochemistry on 10d wound tissue. Scale bar, 100µm. *, $p< 0.05$. Data represented as mean ± sd, **, $p<0.01$, n=4. See also Figure S5.

Figure 7. Model for regulation of BMSCs by the Nrf2/Keap1 pathway and disruption in diabetes

In steady-state, activation of the Nrf2/Keap1 pathway preserves redox metabolism, multipotency and associated features of BMSCs. Nrf2 drives transcription of antioxidants, metabolic modulators and Sox2 to maintain low ROS in BMSCs and maintain multipotency. In diabetes, loss of Nrf2-driven transcription, high intracellular ROS promotes expression of adipogenic genes and leads to commitment of BMSCs to an adipogenic fate.

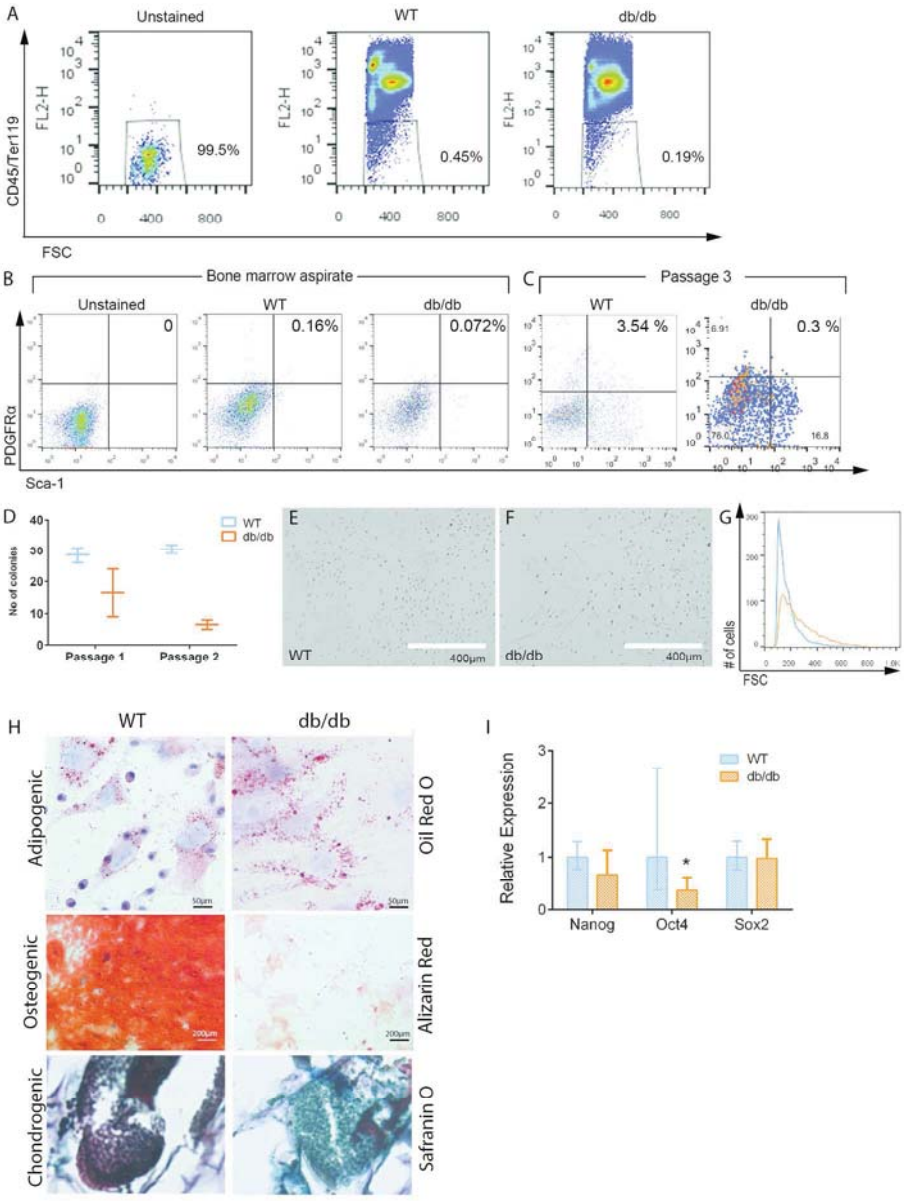

Figure 1

191x254mm (300 x 300 DPI)

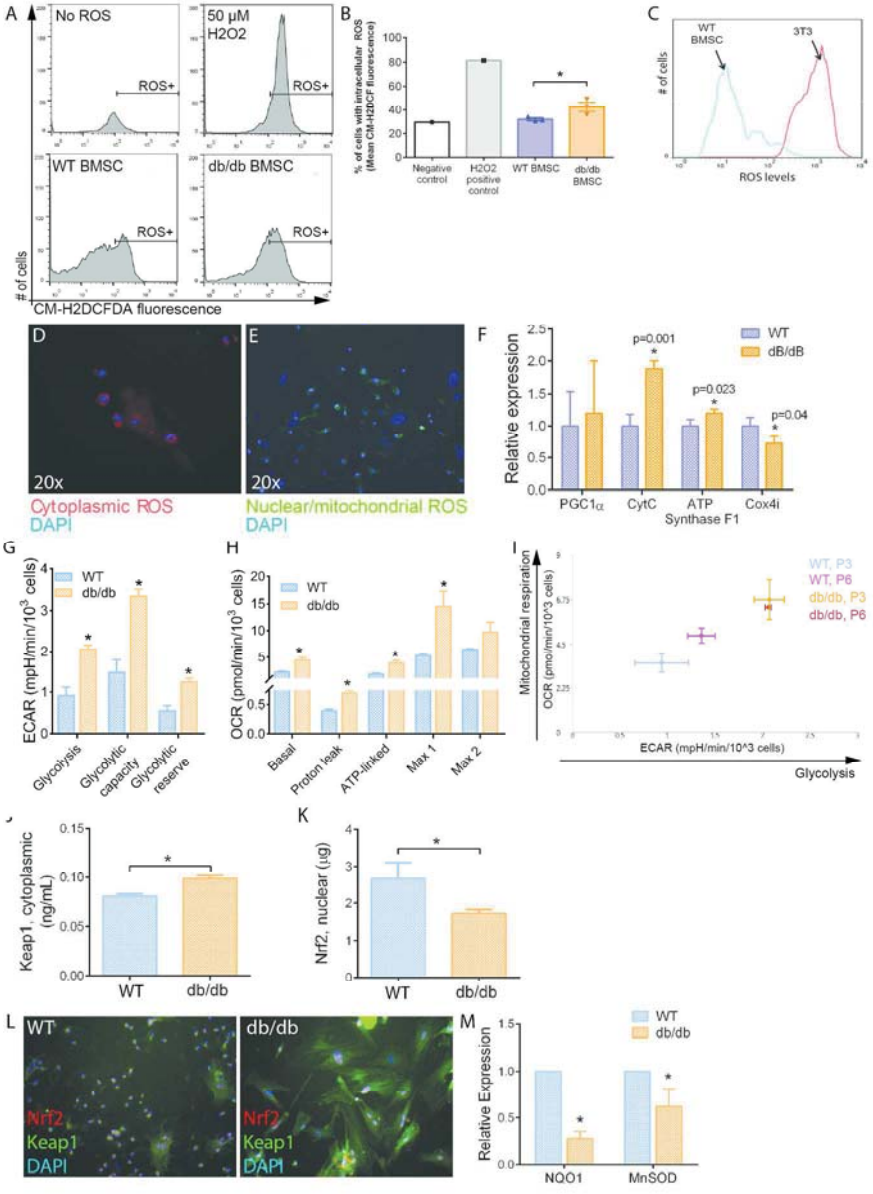

Figure 2

190x254mm (300 x 300 DPI)

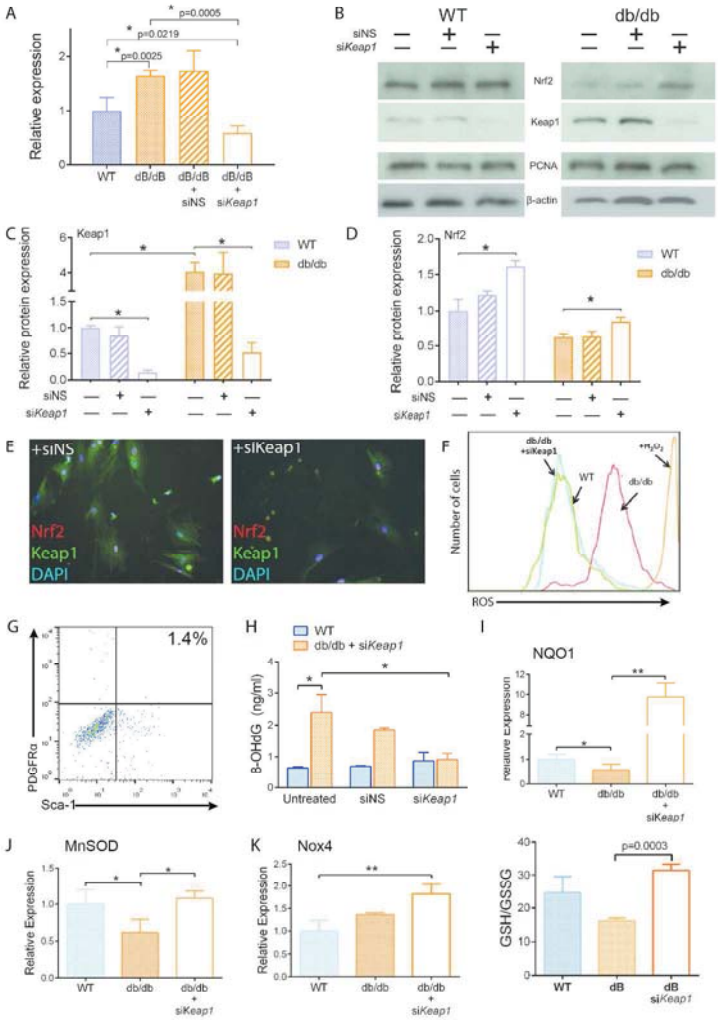

Figure 3

215x279mm (300 x 300 DPI)

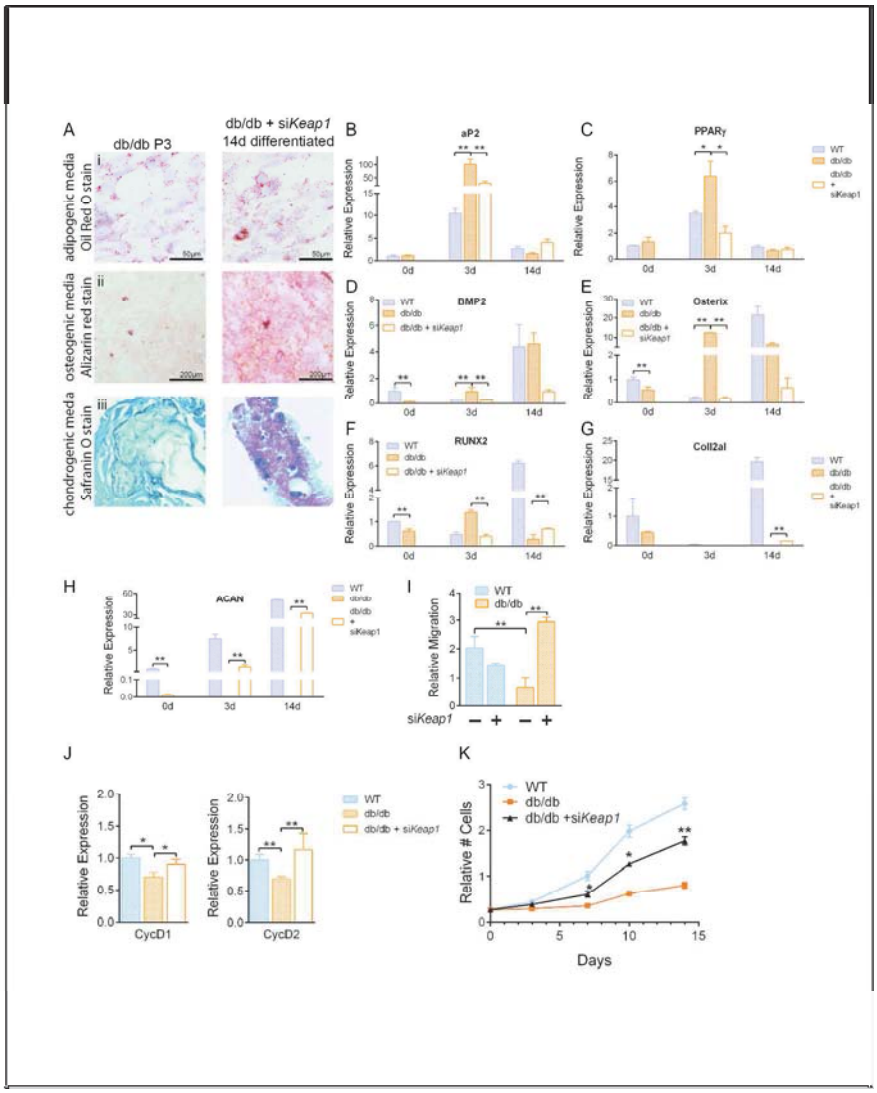

Figure 4

243x263mm (300 x 300 DPI)

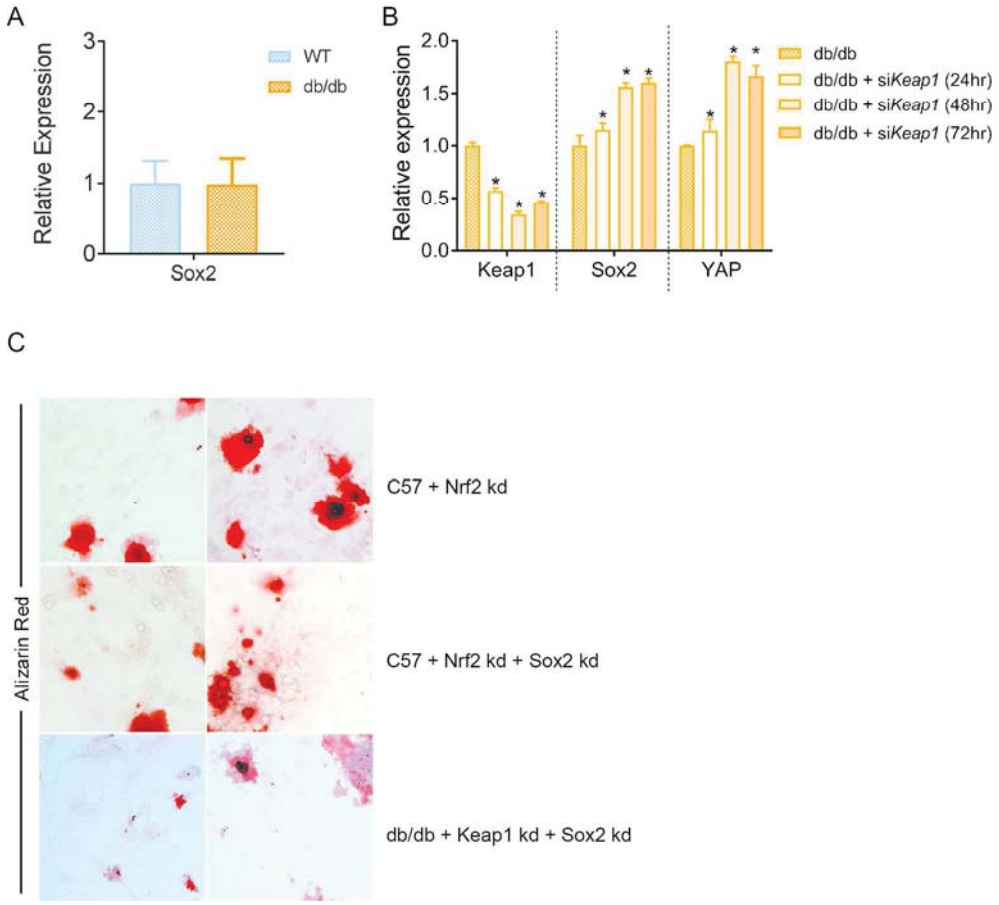

Figure 5

163x146mm (300 x 300 DPI)

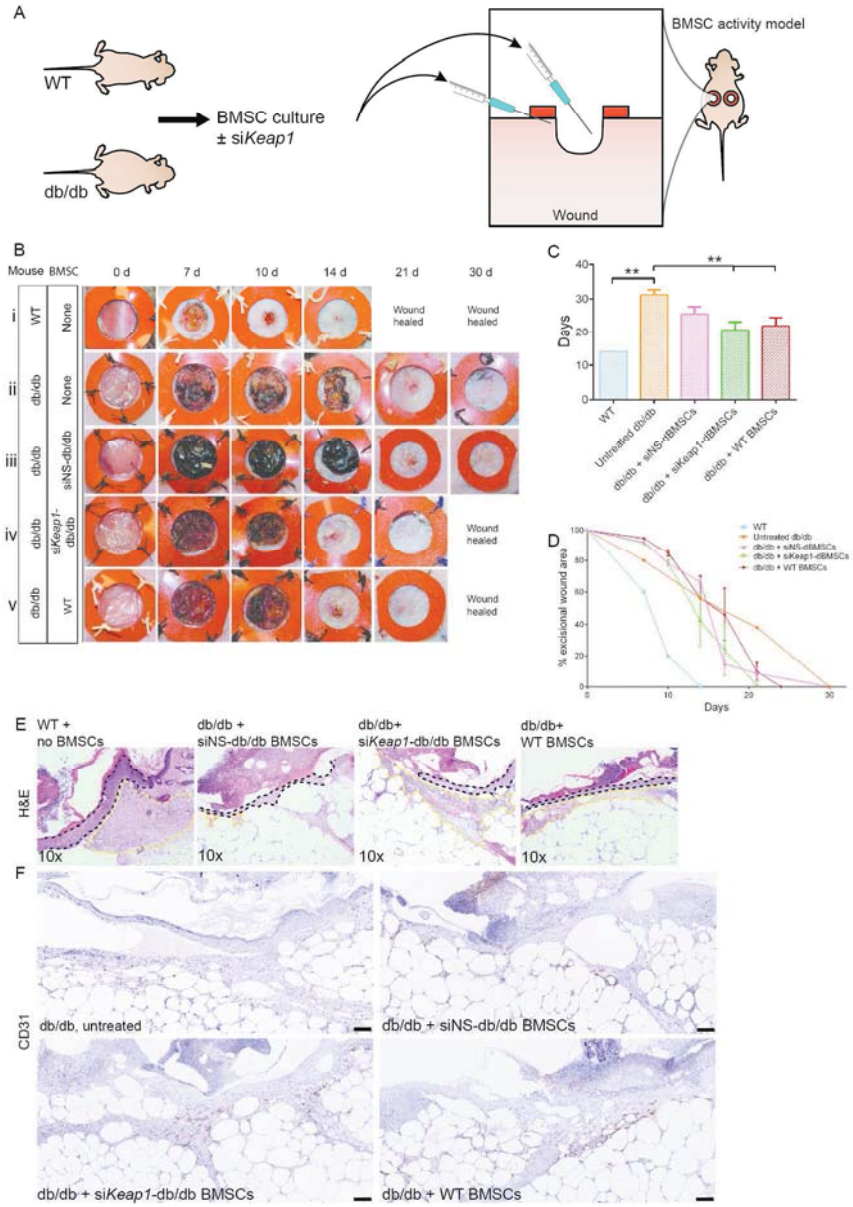

Figure 6

185x242mm (300 x 300 DPI)

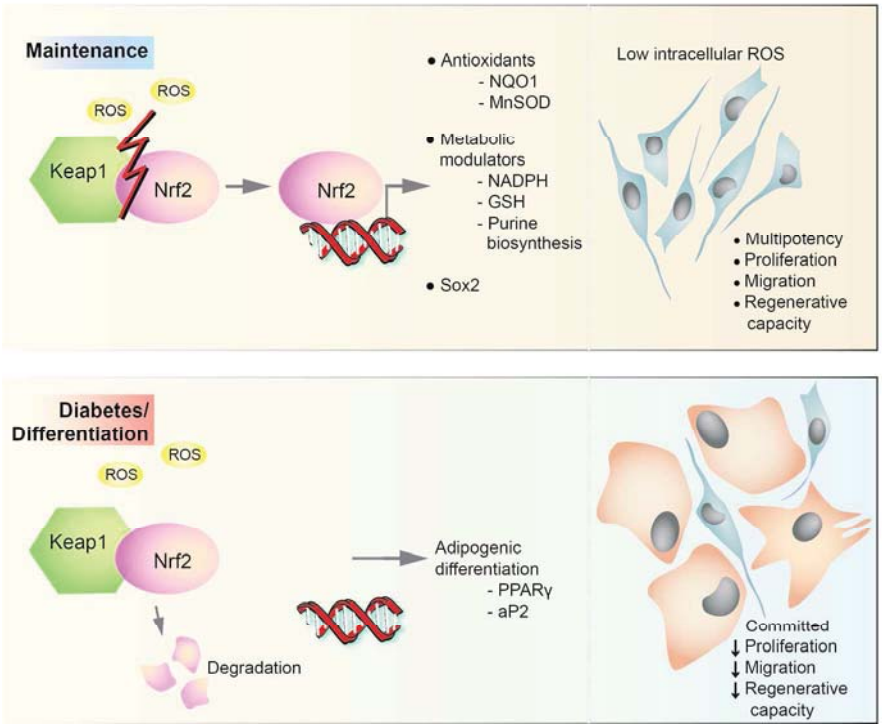

Figure 7

244x190mm (300 x 300 DPI)

Supplemental Materials

Dysregulation of Nrf2/Keap1 redox pathway in diabetes affects multipotency of stromal cells

Piul S Rabbani, Marc A Soares, Sophia G Hameedi, Rohini L Kadle, Adnan Mubasher, Maria Kowzun, Daniel J Ceradini

Supplemental Figures

SUPPLEMENTAL FIGURES

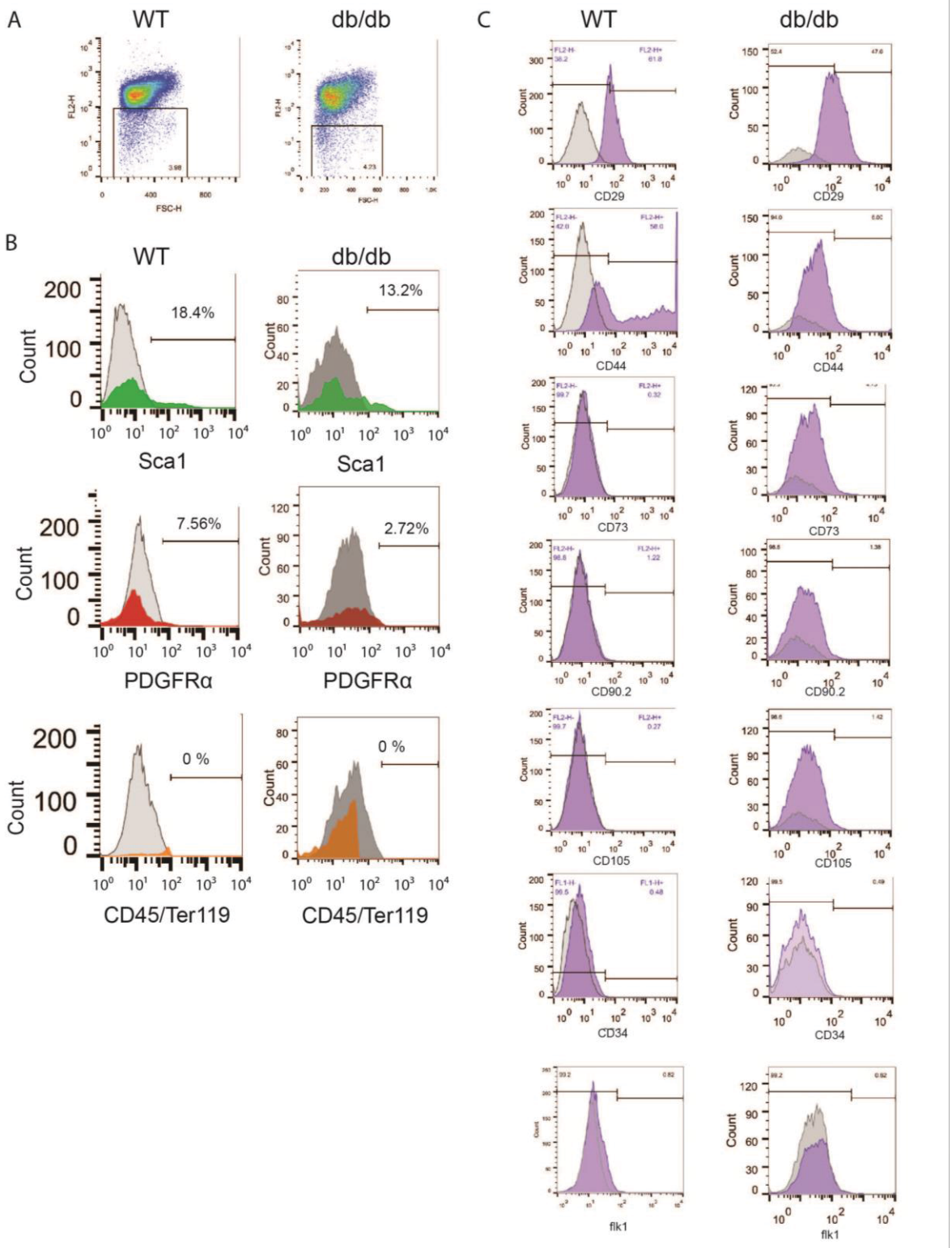

Figure S1. Related to Figure 1. Cell surface marker analysis of passage 3 BMSCs.

A) Passage 3 bone marrow was stained with CD45-PE and Ter119-PE to identify cells with and without these hematopoietic lineage markers. B) Single color stains on CD45-/Ter119- P3 cells. C) Single color stains as indicated.

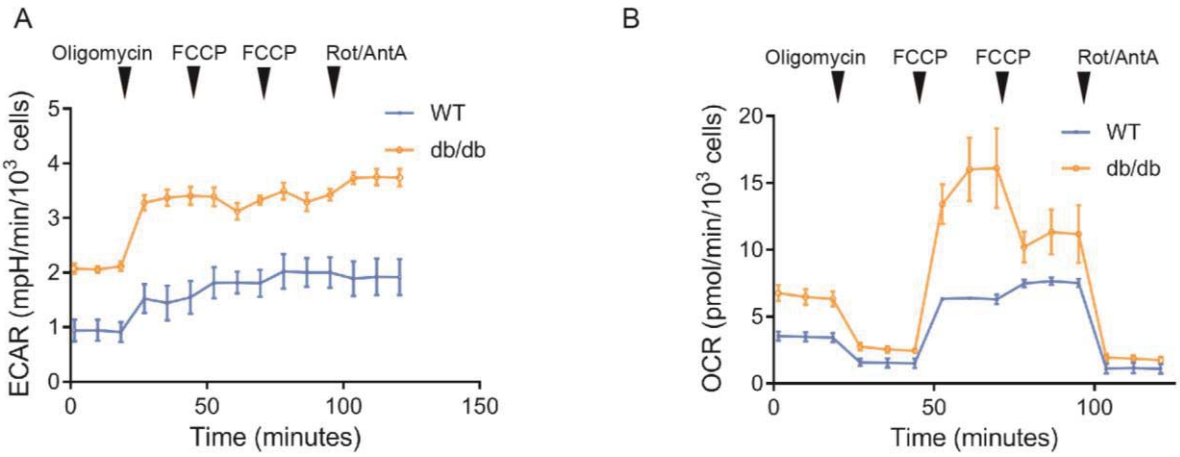

Figure S2. Related to Figure 2. Energy profiles of BMSCs with mitochondrial inhibitory analysis.

A) Extracellular acidification rate (ECAR) analysis, and (B) oxygen consumption rate (OCR) analysis in WT and dBMSCs. Baseline and measurements after addition of oligomycin, FCCP (2 separate injections to detect maximal mitochondrial respiration), and rotenone/antimycin A are shown.

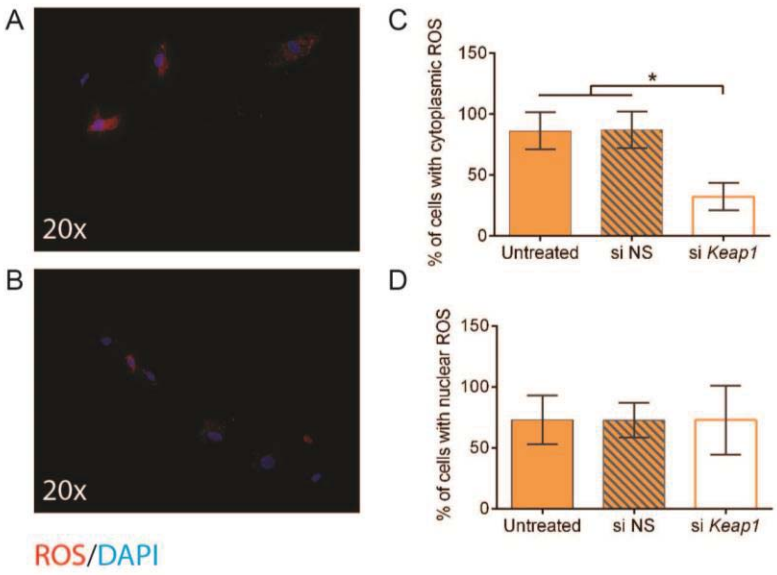

Figure S3. Related to Figure 3. ROS decreases in dBMSCs with *Keap1* inhibition.

A) Cytoplasmic and (B) nuclear ROS imaging following si*Keap1* transfection in dBMSCs. C, D) Quantification of cells displaying ROS. At least 3 fields at 20x were used for counting $DAPI^{+}ROS^{+}$ and $DAPI^{+}ROS^{-}$ cells.

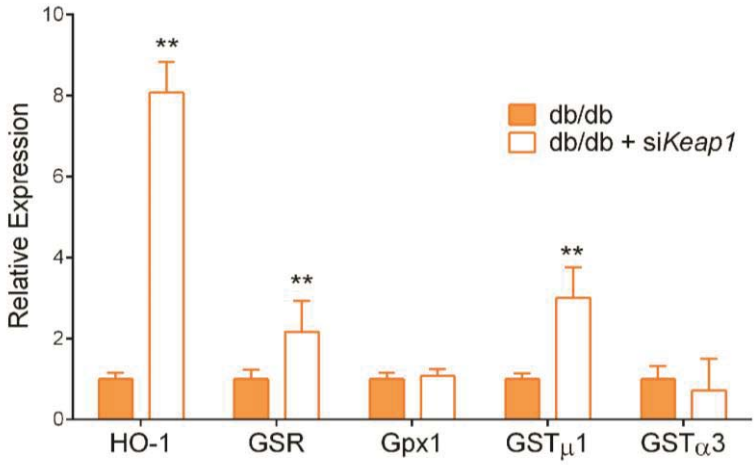

Figure S4. Related to Figure 3. Antioxidant gene expression changes in db/db BMSCs following silencing *Keap1*.

Relative expression of antioxidant genes, downstream of Nrf2, 24 hours after si*Keap1* transfection in db/db BMSCs.

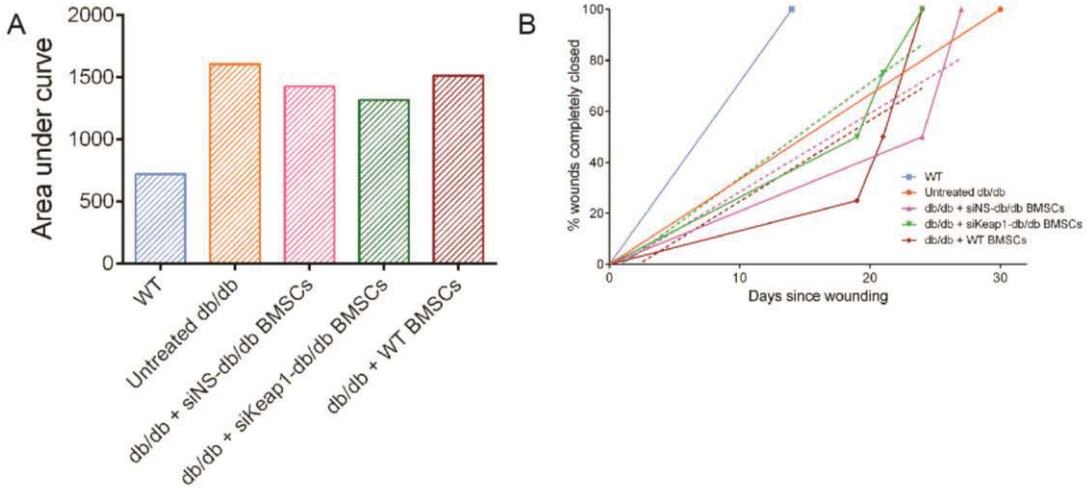

Figure S5. Related to Figure 5. si*Keap1*-db/db BMSCs accelerate diabetic wound healing and lower pathologic wound burden.

A) Wound burden (area under curve of Figure 5D). B) Wound healing pace of diabetic wounds with seeded BMSC as indicated. Color of dashed lines correspond to BMSC treatments in key, and slope indicates rate of closure.